CHAPTER

20

IONOSPHERE AND THERMOSPHERE RESPONSES TO EXTREME GEOMAGNETIC STORMS*

Anthony J. Mannucci, Bruce T. Tsurutani
California Institute of Technology, Pasadena, CA, United States

CHAPTER OUTLINE

1 HISTORICAL BACKGROUND

Decades of research into ionospheric behavior have produced a consensus understanding of major perturbations that can occur. This understanding is far from complete, particularly considering variations at the mesoscale and finer. However, this understanding forms a basis for how to extrapolate ionospheric behavior to extreme events. Our focus is on those aspects of ionospheric extremes that cause large total electron content (TEC) values to appear during daytime. Affected technological systems include navigation (e.g., global navigation satellite systems), HF communications systems, and radar.

Extreme Events in Geospace. https://doi.org/10.1016/B978-0-12-812700-1.00020-0

Ionospheric extremes that are "societally relevant" can fall into these two categories when considering TEC: large TEC values, in particular, that arise suddenly, and spatial TEC gradients. The former can cause navigation errors for a variety of systems and will also degrade radar range values. Spatial TEC gradients are of a particular concern to wide-area satellite-based navigation augmentation systems, such as the U.S. Wide Area Augmentation System (WAAS) used in commercial and private aviation (Sparks et al., 2011a,b; Enge et al., 1996). WAAS is designed to protect its aircraft navigation users from *hazardously misleading information* (HMI) that can arise from inadequate characterization of ionospheric spatial structure. Vulnerability to HMI increases in the presence of localized ($\sim$100 s of km or smaller) TEC enhancements or depletions. We focus in this chapter on mid-to-low latitudes (e.g., below 50° latitude) where many technology systems are affected.

When discussing ionospheric impacts, it is important to clearly define what is meant by "storm" in this chapter. Other chapters refer extensively to geomagnetic storms, which are of course associated with space weather impacts. "Ionospheric storms" refers to the ionospheric effects associated with geomagnetic activity. The root cause of ionospheric storms is generally accepted to be the same root cause of geomagnetic storms: enhanced energy input from the solar wind due to increased interplanetary magnetic field magnitudes, increased plasma speed, densities, and temperatures. Significant ionospheric variability may also be associated with other drivers, such as the lower atmosphere, although the largest effects likely arise from solar activity. It is important to understand the distinction between these geomagnetic and ionospheric storm types, despite their common cause, because geomagnetic storms are often associated with specific variations of geomagnetic indices. Ionospheric storms are general perturbations of the upper atmosphere that may or may not correlate well with variations in geomagnetic indices. Ionospheric storms have their own character and evolution, but it is widely believed that extreme geomagnetic storms will correlate with extreme ionospheric behavior.

To understand and plan for how technological systems may be affected by extremes, it is useful to have approximate quantitative estimates of key geophysical variables. One encounters the problem that there are limited numbers of observations from which to derive such estimates, as the observational record of extremes is likely incomplete. This limitation can often be partially overcome by focusing on the physical ideas, possibly in simplified form, from which reasonable extrapolations can be made. Extrapolations should not be made solely from the data, without this understanding. Theoretical simplifications can provide a form of confirmation: if approximate simple calculations cannot justify the expectation of extreme behavior, then confidence in more complex calculations is limited, particularly when physical justification is absent. Ultimately, a realistic and complex calculation could in theory provide the best answer, but with very limited observations, this can be difficult to justify. Thus, an emphasis on physical ideas is the focus of this chapter. We indicate where more complex calculations are needed and useful. Our discussion occurs with reference to the Carrington storm of 1859, where the measure of geomagnetic storm intensity given by the Dst index has been estimated to be as large as -1760 nT (see Chapter 7 of this volume), compared to -451 nT for the October 30, 2003, storm discussed in detail here (see Mannucci et al., 2005a, 2008 for discussions of superstorms from Solar Cycle 23).

It is well known that the largest storm-time TEC values generally occur during daytime (Mendillo and Klobuchar, 1975). This is in accord with the well-known diurnal cycle of ionospheric electron density whereby electron-ion pairs are created by photoionization, a process of plasma *production* that increases plasma density in a volume of the atmosphere (Schunk and Nagy, 2009). During disturbed periods, increased plasma density compared to quiet conditions is known as the *positive* ionospheric

storm phase (Mendillo and Klobuchar, 1975). Initially, it was not understood how plasma density could increase during geomagnetic storms given that plasma production rates should not be higher during the storm; increased ionizing radiation due to solar extreme ultraviolet (EUV) fluxes are not associated with the storms themselves, but are rather associated with the possible solar flares that may have occurred several days earlier. Eventually, it was realized that geomagnetic storms did not increase EUV production significantly at middle and lower latitudes, where the largest increases occur. (At auroral to middle latitudes, production due to particle precipitation does increase, but this increase is not the focus of our report). Rather, increased TEC occurs despite constant solar ionizing radiation, because of decreased plasma recombination rate (loss). We will show how this basic physical idea permits us to set reasonable "benchmarks" on what can occur during extreme conditions.

For decreased loss to be a cause of the storm-time TEC increase requires that the "nominal" production rate due to daytime photoionization is sufficiently large to account for the TEC increase over time. If plasma is produced in the absence of recombination, can TEC increase as rapidly as is observed? In the next section, we quantitatively explore this idea.

2 ELECTRIC FIELDS AND THE CREATION OF LARGE TEC INCREASES

An example of a large column-integrated electron density increase is shown in Fig. 1 (Mannucci et al., 2005b). This figure shows the integrated electron content (IEC) above the CHAMP satellite orbiting at 400 km altitude as measured by the dual-frequency GPS receiver onboard the satellite. The dual-frequency measurements of delay are related to the IEC via the following formula (Stephens et al., 2011):

$$\Delta_{12} = 40.3\,\mathrm{IEC}\left(1/f_2^2 - 1/f_1^2\right) \tag{1}$$

where Δ_{12} is the measured delay difference between the two GPS frequencies expressed in meters, f_1 is the L1 GPS frequency (1.5754 GHz), f_2 is the L2 GPS frequency (1.2276 GHz), and IEC is expressed in number of electrons per square meter (1 TEC unit is 10^{16} el/m^2). A constant interfrequency bias (IFB) for the receiver and each of the GPS satellites must generally be estimated for these types of measurements (Mannucci et al., 1998, 1999).

The blue trace in Fig. 1 is the prestorm IEC estimate above the satellite. There is often more than a single trace at a given time indicating tracking of more than one GPS satellite by the receiver, above the elevation angle cutoff of 40° used in this analysis. The next pass of the satellite, shown in red, is the first daytime pass following storm commencement, which is near to the time when a southward solar wind magnetic field B_z component reached the magnetopause (see Mannucci et al., 2005b for details). We note that this October 30, 2003, storm occurs during the recovery period of an intense storm occurring on the preceding day. The next and last pass of the satellite shown in this figure is the black trace, where the largest IEC values are observed at magnetic dipole latitudes near −30°. To summarize, in the span of ~200 min, the global structure of electron density above 400 km altitude undergoes very large changes, including a factor of 13 IEC increase (from 26 to 335 TECU) at −28° dipole latitude.

Because the pre-storm (Fig. 1, blue) and post-storm (black and red) satellite passes traverse North America, we can find GPS receivers near the satellite ground tracks to validate and compare with the IEC. We expect that well-calibrated IEC/TEC measurements measured from ground receivers near to the satellite overpass will exceed IEC measurements from CHAMP. To the mid-bottom right of the

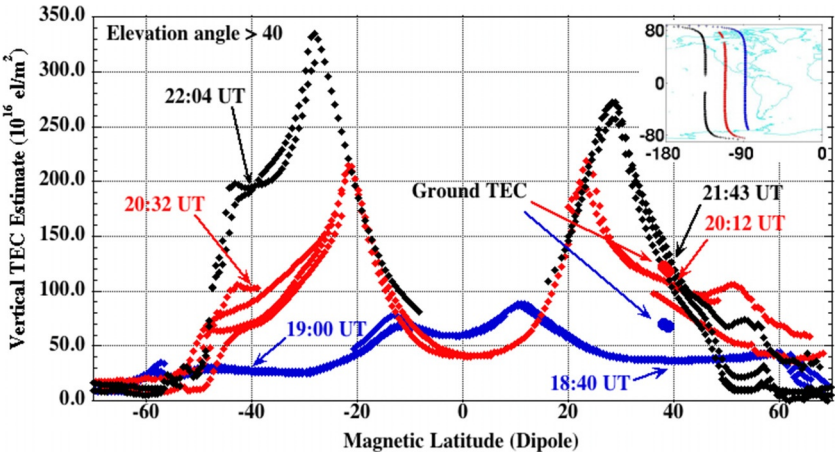

FIG. 1

Vertical integrated electron content (IEC) measured above the CHAMP satellite at 400 km altitude for daytime passes on October 20, 2003. Equatorial solar local time is 1300 LT.

From Mannucci, A.J., et al., 2005. Hemispheric daytime ionospheric response to intense solar wind forcing. In: Burch, J.L., Schulz, M., Spence, H. (Eds.), Inner Magnetosphere Interactions: New Perspectives From Imaging. In: Geophysical Monograph, vol. 159. American Geophysical Union, New York, pp. 261–275. doi:10.1029/159GM20; Mannucci, A.J., Tsurutani, B.T., Iijima, B.A., Komjathy, A., Saito, A., Gonzalez, W.D., Guarnieri, F.L. Kozyra, J.U., Skoug, R., 2005, Dayside global ionospheric response to the major interplanetary events of October 29–30, 2003 "Halloween Storms." Geophys. Res. Lett. 32(1), L12S02. https://doi.org/10.1029/2004GL021467.

figure, near 40° latitude, are indicated two vertical TEC estimates from ground-based receivers in North America near the time of the CHAMP overflights. The ground-based TEC is calibrated using the Global Ionospheric Mapping (GIM) technique (Mannucci et al., 1998). Pre-storm, we find that TEC is approximately twice the IEC from CHAMP. During the storm, TEC and IEC are approximately equal. The pre-storm ratio suggests that approximately half the TEC comes from electrons above 400 km altitude, which is reasonable based on "typical" mid-latitude electron density profiles, as can be verified using the International Reference Ionosphere (IRI) model for example (Bilitza et al., 2014).

During the storm (red trace), the IEC has grown to be ~90% as large as the ground-based TEC (red circle near 40° latitude versus the closest CHAMP value). Thus, most of the plasma is above the altitude of the satellite after storm commencement. Considering pre- to poststorm conditions, comparison with ground-based TEC is strongly suggestive of plasma upward motion. The Halloween storm is an intense example of a *positive storm effect* that occurs during the main phase of a geomagnetic storm (Mendillo, 2006; Tsurutani et al., 2004). This daytime positive effect is generally caused by dawn-to-dusk (eastward during daytime) electric fields of magnetospheric origin, so-called "prompt penetration electric fields" (PPEF). The resulting $\mathbf{E} \times \mathbf{B}$ drift convects the plasma vertically upward. For fixed eastward field, such drift will be maximum near the geomagnetic dip equator where $\mathbf{B}$ is close to horizontal (north-south direction).

$\mathbf{E} \times \mathbf{B}$ drift speeds v are given by: $v = \mathbf{E} \times \mathbf{B}/B^2$ (Kelley, 2009). Storm-time values of electric field often reach ~1 mV/m (Huang et al., 2005) or higher. The magnetic field magnitude $\mathbf{B}$ is ~30,000 nT

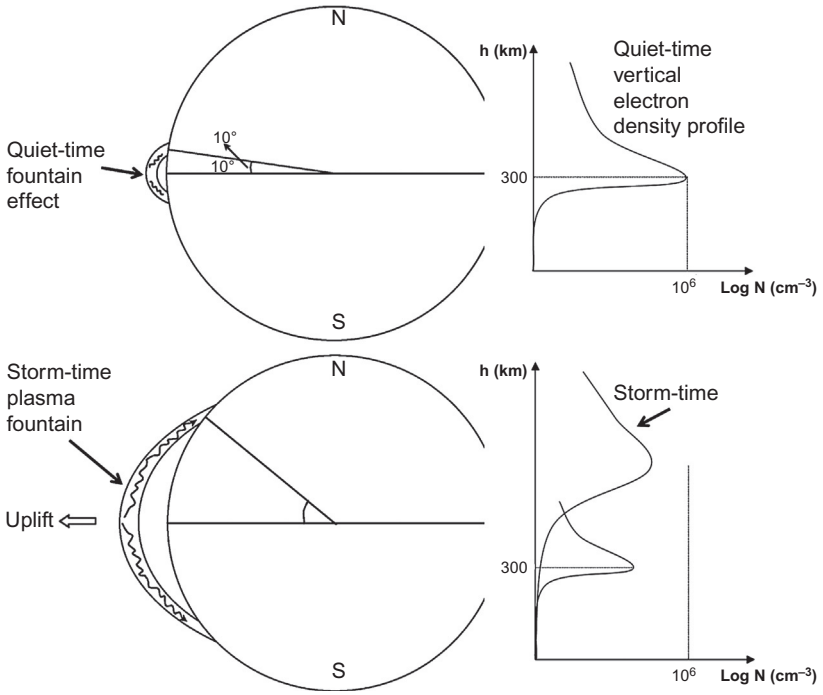

FIG. 2

A schematic description of the ionospheric superfountain created by large prompt penetration electric fields. Left: increased vertical transport broadens in latitude the region of the equatorial fountain effect. Right: schematic representation of vertical plasma uplift during storm conditions.

Based on Tsurutani, B., et al., 2004. Global dayside ionospheric uplift and enhancement associated with interplanetary electric fields. J. Geophys. Res. Space Phys. 109(A), A08302. doi:10.1029/2003JA010342.

near the dip equator at altitudes near 300 km. This leads to velocities in the range ~41.7 m/s, or ~150 km/h, sufficiently large to rapidly move plasma from altitudes where production rates are largest (~130–150 km) to altitudes where production rates are factors of 10 lower (~250 km). These vertical velocities suggest the uplift mechanism is amply capable of producing the observed TEC increases. The modified TEC structure has been referred to as an ionospheric "superfountain" effect by analogy to the "fountain effect" that causes the nominal low latitude TEC structure (equatorial ionization anomaly). The superfountain is schematically depicted in Fig. 2. Increased plasma vertical transport speeds and subsequent plasma diffusion along magnetic field lines contribute to increased ionization at latitudes more poleward than nominal conditions.

To gain further insight into positive phase storms, we use published production rates to calculate the column density of electrons generated per hour to compare with the measurements of Fig. 1. The result, based on production rates reported by Richards (2014) representative of solar maximum conditions on March 17, 1990, (188 F10.7 Solar Flux Units) is that 383 TECU per hour can be generated considering the three dominant ion species O^+, NO^+, and $O_2{}^+$.

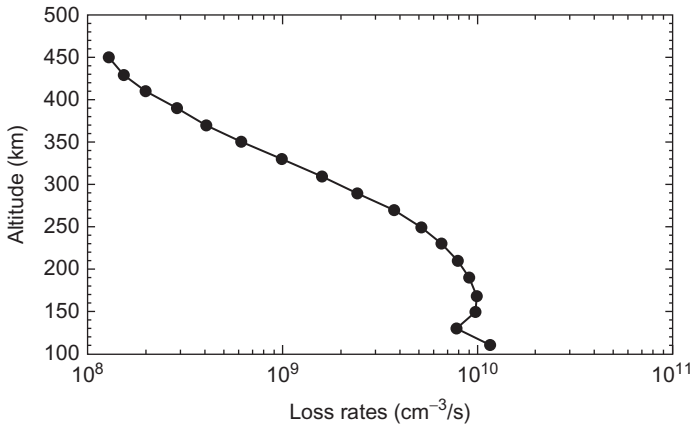

FIG. 3

Ion recombination rates for the three major ion species O^+, NO^+, and $O_2{}^+$, characteristic of solar maximum conditions on March 17, 1990.

Based on the model of Richards, P.G., 2014. Solar cycle changes in the photochemistry of the ionosphere and thermosphere. In: Modeling the Ionosphere-Thermosphere System, vol. 89. John Wiley & Sons, Ltd, Chichester, pp. 29–37.

These ion production rates are generally consistent with the IEC increases from Fig. 1, which can be explained by ion production of ~100–200 TECU/h, depending on how many ions are transported above CHAMP altitude. Using ion production rates alone to understand the ionospheric response to the extreme Halloween 2003 storms is overly simplistic because it does not account for recombination chemistry that occurs as the ions move upward to regions of lower concentrations of neutral and ion species. The consistency between the production rates and the measured TEC increases is suggestive, however, that reduced plasma recombination (loss) is sufficient to explain the observed TEC increases.

Ion recombination rates versus altitude characteristic of solar maximum, also based on Richards (2014), are shown in Fig. 3. The steep fall-off of recombination rates with altitude is why TEC can increase dramatically from upward drifting plasma. We note that photochemical ion production rates have a similar altitude dependence—peaking near altitudes between 120 and 150 km. As is well known, vertical transport of photochemically produced ions counteracts the sharp fall-off of plasma density with altitude, producing a peak plasma density in the F-region at altitudes near ~350 km (Rishbeth and Garriott, 1970).

A notable feature of Fig. 1 is the *reduced* TEC between −10° and 15° dipole latitude in the second pass shown (red trace). Vertical TEC reduction, particularly at such low latitudes, is not consistent *per se* with an uplift mechanism. However, the reduced TEC could be due to transport associated with the equatorial fountain effect, as first modeled by Moffett and Hanson (1965). (See also Hanson and Moffett, 1966). Evidence that vertical drift reduces TEC near the equator is found in the quiet-time blue trace that shows the "nominal" equatorial ionization anomaly. The modeling work by Moffett and Hanson (1965) and others subsequently (Anderson, 1973) reproduce this feature associated with vertical and horizontal plasma transport away from the geomagnetic equator (see Fig. 2).

Detailed modeling of the ionospheric superfountain using SAMI-2 (Huba et al., 2000) has been reported (Tsurutani et al., 2007). Such modeling confirms that transport can reduce equatorial TEC

under the strong uplift conditions characteristics of intense geomagnetic storms. Impactful thermospheric responses are likely as well, as we discuss below.

Heelis et al. (2009) have discussed another mechanism for TEC increases at higher middle latitudes (40° geomagnetic and higher) that are caused by the expansion of the high latitude convection pattern. These increases are related to horizontal plasma flows resulting from sunward plasma convection from dusk towards noon, "piling up" plasma at afternoon local times. As discussed in Chapter 21, for the largest storms, the expanded convection pattern flows will likely merge with the lower latitude increases due to the superfountain, forming the dramatic increases observed in the 2003 Halloween storms (Fig. 1), affecting the entire low-to-middle latitude ionosphere. Large plasma density gradients are likely to result from this combination of plasma motions, as has been reported by radars and GPS receivers in the Eastern North American sector (see Heelis et al., 2009 and references therein).

The CHAMP data (Fig. 1) show somewhat divergent TEC values among the multiple storm-time traces (red and black) appearing between 40° and 60° latitude (north and south). Multiple vertical IEC values at a single time are due to the IEC being derived from different GPS satellites above CHAMP. These divergent values reveal that the electron density distribution above CHAMP is not azimuthally symmetric, and that slant IEC depends on the direction of the line of sight between CHAMP and the individual transmitting GPS satellites. Such azimuthal dependence is likely due to horizontal TEC gradients above the satellite. Thus, the extreme ionospheric response we study is not only characterized by large electron density and TEC increases, but also larger horizontal gradients of TEC, which has a major impact on GPS positioning (see Chapter 23).

The physical mechanism by which electric fields "penetrate" to low latitudes has been investigated in several theoretical studies (e.g., Nopper and Carovillano 1978; Rothwell and Jasperse, 2006). Not all aspects of this "penetration" appear to be understood (e.g., Kikuchi et al., 1978), but much of the theoretical work is based on achieving consistency between magnetospheric Region-1 field aligned currents, the cross polar cap potential, and ionospheric conductance globally, dominated by E-region conductance (altitudes 100–120 km). Shielding by Region-2 currents was thought to mitigate much of the effect within 1 h for typical storms (Fejer and Scherliess, 1995; Richmond, 1995), but studies have clearly shown long-duration penetration for superstorms (Mannucci et al., 2008; Huang et al., 2005). It is appropriate to suggest that extreme geomagnetic storms will expose the low latitudes to very large electric fields of multi-hour duration with minimal shielding. Lakhina and Tsurutani (Chapter 7) suggest that an extreme storm may have a main phase lasting up to 24 h. The implications on dayside uplift for such an extended duration has not been investigated in the ionosphere to our knowledge, but would be important to pursue with detailed modeling and theory.

2.1 EQUATORIAL PLASMA IRREGULARITIES AND SCINTILLATION

As discussed in Chapter 1, a major technological impact from the Earth's upper atmosphere is the formation of turbulence or irregularities in the ionosphere that results in scintillation and possibly signal loss of radio waves used for communications, navigation, and radar purposes. It is reasonable to ask whether the same PPEFs that cause large daytime TEC increases may also lead to the formation of irregularities and whether their intensity may increase during extreme storms. We focus here on equatorial scintillation because this is most directly related to PPEF. Although there is little existing literature on the subject of extreme effects, extrapolation based on existing observations and theory is a reasonable approach.

Equatorial scintillation during nominal conditions is primarily a dusk to premidnight phenomenon. It originates from the Rayleigh-Taylor instability, when lower-than-normal plasma densities are situated below larger plasma densities aloft (Abdu, 2012). The buoyancy of the lower layer tends to lift plasma into the denser layer and large plasma depletions (or "bubbles") form in the F-region (altitudes above 300–400 km). The walls of the plasma depletions whose walls consist of irregularly structured plasma. An association of equatorial scintillation with the TEC increases due to PPEF is indirect. In fact, the dawn-to-dusk directed electric field on the dayside will lead to downward plasma convection on the nightside, tending to suppress the instability at night during the storm main phase when PPEF is active. However, as discussed below, intense storms have been found to destabilize the midnight ionosphere after the main phase is over, due to either a disturbance dynamo electric field, which raises the plasma at night, or over-shielding (described below). Because irregularities are associated with plasma depletion, and depletion cannot continue past zero plasma, it is unclear how the intensities of specific equatorial depletions increase due to extreme events, even though based on analysis of intense storms, the extent of equatorial scintillation is likely to occupy a broad range of post-sunset local times, as discussed below.

Basu et al. (2001a) studied two intense storms in 1999 and found increased equatorial scintillation associated with PPEF, in a range of local times extending to the postmidnight sector. Yeh et al. (2001) also found that, for the intense geomagnetic storm of October of 1999, scintillation extended past midnight into the predawn hours. Such a broad local time region of increased scintillation during extreme storms is a reasonable extrapolation based on our current understanding of the mechanisms. Basu et al. (2001a) hypothesized that the post-midnight scintillation was related to an apparent "driver" of scintillation: rapid decrease in the Dst index, indicating rapid changes in stormtime magnetospheric convection. This rapid convection increase, likely leading to efficient electric field penetration to low latitudes, destabilized the ionosphere at dusk. The later postmidnight irregularities were due to this destabilized region rotating to later local times. The intriguing results of Basu et al. (2001a) were reaffirmed in a study of the October and November 2003 superstorms (Basu et al., 2007) suggesting the robustness of the result across storm intensities. These works find significant dusk-time depletions occuring during rapid decreases in the Dst index. This association of irregularities with Dst behavior is further corroborated for the "Bastille Day" July 14, 2000, superstorm (Basu et al., 2001b). At times when Dst is not decreasing rapidly, there is less enhancement of dusk-time equatorial scintillation, and less destabilization of the ionosphere. Understanding the physical processes underlying why the rate of Dst variation affects equatorial scintillation, and how this would translate to extreme events, is an important area of future research.

As mentioned above, suppression of equatorial scintillation has also been reported associated with geomagnetic storms. Suppression can be due to downward plasma motion from the PPEF, which is directed westward at night. Based on the physical mechanism, we would expect this main-phase suppression to continue into extreme events. The review by Abdu (2012) discusses both suppression and increased occurrence of equatorial scintillation associated with disturbance electric fields. Increased occurrence is caused by the transient phenomenon of *over-shielding* where shielding electric fields that developed during the main phase create nighttime dusk-to-dawn electric fields that are opposite to the PPEF direction (see Fig. 8 in Chapter 10). This results in upward nighttime plasma drift, which is conducive to irregularity formation. Extreme events would likely lead to similar over-shielding cases. Yeh et al. (2001) emphasize disturbance dynamo electric fields as the source of midnight uplift. Carter et al. (2014) discuss the more common suppression case using the geomagnetic K_p index as a

predictive parameter. Extreme storms may bring enhancement of scintillation across a broad range of local times, as discussed above.

Scintillation will of course occur at other latitudes as well. High-latitude scintillation is quite common and can occur during relatively weak geomagnetic storm conditions. Middle-latitude scintillation (below ~60° geomagnetic latitude) is virtually absent except during geomagnetic storms, where its occurrence is closely tied to the expansion of the high latitude convection pattern. These topics are covered in Chapter 23.

3 THE ROLE OF ION-NEUTRAL COUPLING

Tsurutani et al. (2007) were the first to report a possible connection between the neutral atmosphere and strong plasma uplift. In that study, it was shown that the rapid upward motion of O^+ ions due to PPEF can cause neutral oxygen (O) to be uplifted also, due to ion-neutral drag. These authors suggested that above ~400 km altitude, the neutral thermospheric density could substantially increase such that it can have a major impact on satellite drag. Because we now believe that PPEF during superstorms is an expected phenomenon, satellite drag impacts due to ion uplift will be a feature of extreme storms, in addition to the thermospheric expansion caused by temperature increases that has been studied extensively (e.g., Rees, 1995. See also Chapter 21).

A first-order understanding of the expected neutral density increase can be made from simple momentum exchange considerations. Momentum is imparted to the neutrals via collisions according to the following equation (e.g., Baron and Wand, 1983; Killeen et al., 1984; Brekke and Rino, 1978):

$$\rho_n \frac{\partial U}{\partial t} = \rho_i \nu_{in} (V_d - U) \tag{2}$$

where U is the vertical neutral velocity imparted by the uplifting ions, ρ_n is the neutral density, ν_{in} is the momentum transfer collision rate from the ions to the neutrals, and V_d is the vertical uplift velocity. We have numerically integrated Eq. (2) under conditions similar to what occurred on November 10, 1979, when strong EUV emission from the Sun was present near solar maximum, and the F10.7 solar flux value of 367.0 was the largest value recorded after 1960. Values for ion and neutral densities under these conditions were obtained from the International Reference Ionosphere (IRI) model, and the Mass Spectrometer and Incoherent Scatter (MSIS) model (Picone et al., 2002), respectively. The collision frequencies were obtained using the formula of Bailey and Balan (1996), with temperature obtained from MSIS and the further approximation that neutral and ion temperatures are the same. These calculations were run for November 10, 1979, at a low latitude location where vertical uplift is generally largest (0 latitude, −60 W longitude).

Results of the integration are shown in Fig. 4 for two low-latitude electric field values: 1 and 4 mV/m, corresponding to ion vertical drift velocities of 153 and 612 km/h, respectively. The smaller value is large but not extreme and has been observed for several strong storms (e.g., Huang et al., 2005). The larger value is a slight extrapolation from the record value observed near November 9, 2004 (Kelley et al., 2010). We assume neutral vertical velocities are initially zero, and the integration is applied to neutral density parcels starting at 350 km altitude. These calculations are not self-consistent in that densities are not adjusted as the vertical uplift occurs, but are indicative of the consequences to density in an approximate way.

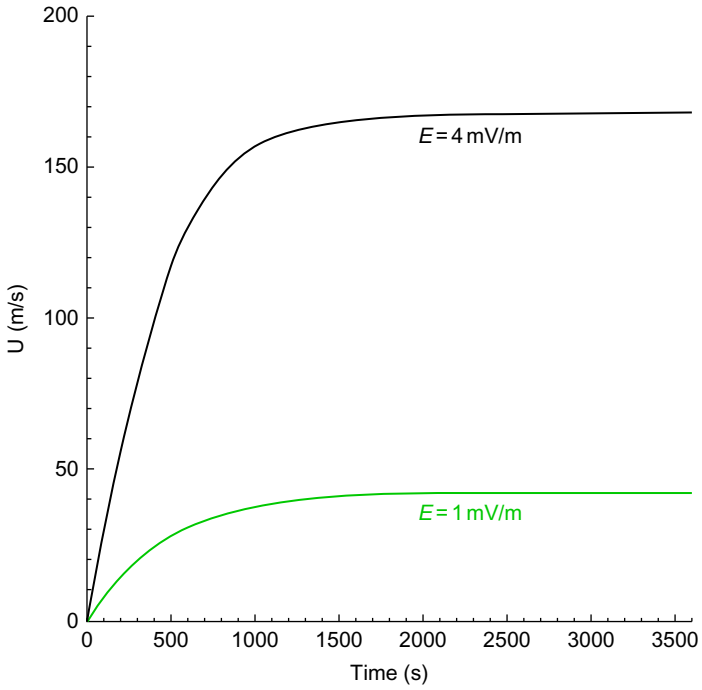

FIG. 4

Neutral velocity versus time according to Eq. (2) for two values of the ion upward velocity.

The calculations show that the "terminal" ion velocity is reached in a matter of tens of minutes for either electric field value. Neutral uplift distances of ~100–400 km are plausible in as little as 1–2 h. Table 1 shows densities, from IRI and MSIS runs, for dominant ion (O^+) and neutral (O) species, respectively. Starting at 350 km altitude, the ratio of the neutral density to its density higher up is calculated (200 km higher in Column 4, and 400 km higher in column 5). Above 350 km, O density is decreasing with altitude, so vertical uplift of O via ion-neutral collision has the potential to increase thermospheric density sufficiently to alter drag forces on a satellite. The ratios in Columns 4 and 5 of Table 1 are upper bounds for neutral density changes that can occur due to neutral uplift. Only a fraction of the neutrals would be uplifted by the ions, because the concentration of the neutral species is much larger than the ion concentration. Nevertheless, these large upper limits are a concern and suggest more detailed time-dependent modeling corresponding to extreme conditions is needed. A modeling study by Zhu et al. (2017) shows that under nominal conditions the thermospheric density at 400 km altitude can change due to vertical plasma drift by 5%–10% at low latitudes. (In this case, the density at 400 km is reduced). It is reasonable to expect much larger changes in neutral density during extreme storms. The vertical motion of the neutrals, in extreme cases, could change horizontal winds as well, due to mass conservation. This topic deserves further research. We note also that, using data from the Defense Meteorological Satellite Program satellites, Tsurutani et al. (2012) found oxygen ion densities could exceed neutral densities at altitudes above ~800 km. Therefore, at higher altitudes extreme storms can create satellite drag increases due to the uplifted ions that exceed neutral drag. This possibility is often over-looked when geomagnetic storms are analyzed.

Table 1 Ion and Neutral Oxygen Densities, From IRI and MSIS Models, Respectively

Altitude	O Density	O^+ Density	Ratio +200 km	Ratio +400 km
100	7.91E+17	0.00E+00	407.4	4270.0
150	2.93E+16	1.37E+11	28.0	274.6
200	8.63E+15	5.38E+11	14.9	139.7
250	3.82E+15	9.36E+11	11.7	105.7
300	1.94E+15	1.41E+12	10.5	91.2
350	1.04E+15	2.00E+12	9.8	82.6
400	5.78E+14	2.59E+12	9.4	76.4
450	3.25E+14	2.14E+12	9.0	71.4
500	1.85E+14	1.49E+12	8.7	
550	1.07E+14	9.97E+11	8.4	
600	6.18E+13	6.78E+11	8.2	
650	3.61E+13	4.75E+11	7.9	
700	2.13E+13	3.45E+11		
750	1.26E+13	2.58E+11		
800	7.56E+12	1.97E+11		
850	4.56E+12	1.53E+11		

Ratios refer to neutral densities between different altitudes, for 200 and 400 km vertical displacements, up to 850 km altitude.

3.1 BUOYANCY (GRAVITY) WAVES

We have neglected gravity and pressure forces in Eq. (2) (e.g., Killeen et al., 1984). Gravity is of most interest here because pressure decreases with altitude, so the pressure gradient force works in opposite direction to the upward collision-induced force. To quantify the effect of gravity, we compare the pressure gradient force due to gravity with the upward force from collisions. The pressure gradient force is estimated using MSIS densities and temperatures and the ideal gas law up to 600 km altitude. Fig. 5 contains the result of the calculation, which compares the acceleration of the neutrals due to collisions with ions with that from the gravity pressure gradient force, and their ratio. While gravity produces larger accelerations, the upward collisional force can reach 5% or more of the gravitational force, especially near altitudes of ~400 km. The net result is likely to be the development of buoyancy waves over a broad low latitude region where the uplift occurs (e.g. see Meng et al., 2015). As neutrals are transported upward, the disruption of hydrostatic equilibrium creates a downward force, decreasing the upward velocity of the parcel that eventually becomes downward. Overshooting produces oscillatory behavior that subsequently displaces neutral parcels aloft, and a vertical wave is launched. Such waves launched by PPEF have been analyzed using the nonhydrostatic GITM model under nominal low-latitude conditions (Zhu and Ridley, 2014).

Thus, significant modification of the neutral and ion densities is plausible for long-duration penetration electric fields. Detailed time dependent calculations are needed with a coupled thermosphere-ionosphere model (e.g., GITM, Ridley et al. 2006) under extreme conditions to understand these effects.

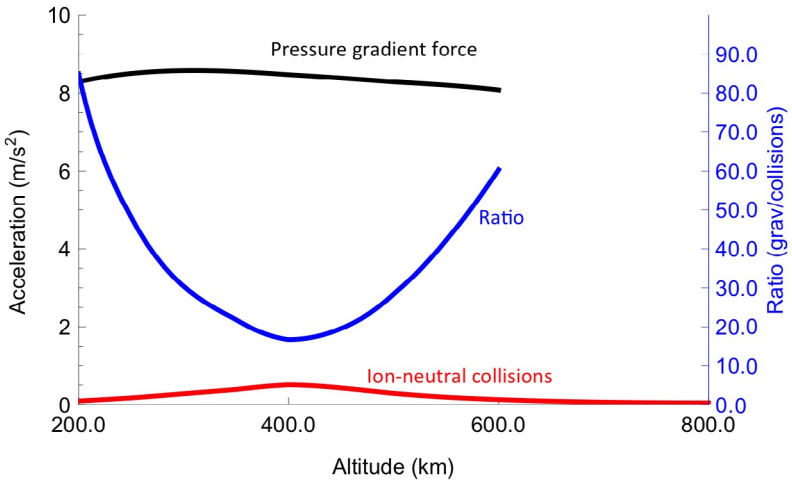

FIG. 5

Acceleration of the neutral oxygen species under the pressure gradient force *(black)* due to gravity and due to collisions with ions *(red)*. The ratio of the two accelerations *(blue)* is on the right axis.

4 EXTREME NIGHTTIME RESPONSES FOLLOWING THE STORM MAIN PHASE (FLORIDA EFFECT)

In this section, we review an unusual ionospheric feature that appeared over Florida in the United States during nighttime of October 31, 2003, in the aftermath of the large geomagnetic storm that occurred on the preceding day. We discuss the nighttime feature in this chapter because we believe it is associated with the extreme conditions associated with that storm, although it is currently unknown whether similar features may be associated with other intense geomagnetic storms.

A practical consequence of what occurred over Florida on October 31 is that it exposed the potential limitations of algorithms associated with the Wide Area Augmentation System (WAAS), designed to assist aviation users of GPS-based positioning systems. Such users require augmentation of the standard GPS signals to meet safety-of-life standards. Users in flight can only officially rely on a single GPS frequency (L1 at 1575.42 MHz) for navigation, until the modernized GPS constellation fully deploys another authorized civil frequency (L5, at 1176.45 MHz) designed for safety-of-life applications. Existing single-frequency WAAS users rely on a dual-frequency ground reference station network of GPS receivers to measure ionospheric TEC. An ionospheric correction is derived from this ground network and broadcast to WAAS users via geostationary satellites above the Continental United States (CONUS). The correction is encoded as a gridded data set, continuously updated, of vertical ionospheric TEC values over a $5° \times 5°$ grid covering the CONUS and extending to Hawaii and Alaska. Because the gridded values are interpolated from irregularly scattered measurements obtained by the ground network, localized TEC enhancements might not be adequately sampled by the reference measurements, leading to incorrect TEC values at the grid point locations. The ionospheric feature that appeared over Florida on October 31, 2003, was so unusual that it exposed potential limitations of algorithms designed to bound the uncertainties of the gridded TEC values. This led to new algorithms

being implemented for WAAS, at significant expense, known as the *extreme storm detector* (Sparks, 2012).

In the remainder of this section, we review characteristics of the nighttime TEC enhancement that occurred on October 31, 2003, known as the *Florida Effect*. Its association with the intense Halloween storms of 2003 is postulated, but its physical origins are currently unknown, so it is not possible to extrapolate with confidence on how such a feature might behave during an extreme storm such as the Carrington event of 1859.

We review the spatial and temporal extent of the localized TEC enhancement based on the work of Datta-Barua et al. (2008). The purpose of that investigation was to estimate the vertical extent of the feature to help understand its physical causes. We can summarize the results as follows:

1. The duration of the enhancement was ~6 h, from 0000 UT to 0600 UT on October 31, 2003 (solar local times of 1900–0100 LT).
2. The horizontal dimensions of the feature reached $\sim 700 \times 700$ km, persisting over a region centered at ~30 N latitude and 80 W longitude.
3. The altitude of peak electron density of the feature is ~160 km higher than the surrounding nighttime background.
4. The feature remained fixed in geographic coordinates until it dissipated at ~0600 UT.

The estimated magnitude of the enhancement based on sampling by the WAAS reference stations and other GPS receivers in its vicinity was ~60 vertical TECU above background vertical TEC values in the immediately surrounding area of ~15 TECU. The resulting slant range delays of up to 20 m are sufficient to cause positioning errors of 40 m or more, depending on details of the GPS satellites being tracked by a specific receiver. WAAS is designed to provide robust bounds for user positioning error, so an undetected positioning error of this magnitude is a significant concern (Sparks, 2012).

Fig. 6 (reproduced from Datta-Barua et al., 2008) shows the horizontal extent of the feature nears its peak at 0330 UT (2210 solar local time) on October 31, 2003. TEC measurements from nearby overflights of the JASON dual-frequency altimeter, capable of measuring TEC below altitudes of 1330 km, suggest that the enhancement was contained entirely below this altitude. TEC data from the SAC-C satellite orbiting at 700 km altitude, which also had a fortuitous nearby overflight, suggest some additional ionization above that altitude. Using typical electron density profiles derived from the IRI model, the peak density of the feature appeared to be near 500 km altitude, in the ionospheric F-region.

The relatively high altitude of the feature and where its peak density occurs argues against the cause being energetic particle precipitation. To achieve large density enhancements from precipitation would require large fluxes of very low-energy particles (<1 eV) that deposit their energy at relatively high altitudes (see Chapter 12 of Jursa, 1985). Such particle populations have never been observed precipitating at such low latitudes.

Of interest in considering extreme space weather is the cause of the Florida Effect feature. Associating this feature with the preceding ionospheric storm, where the largest TEC increases are due to PPEF, suggests that the ultimate source of ionization could have originated in the daytime and that this feature is a result of slow recombination of daytime plasma. For the ionospheric superfountain discussed in the previous section, we found that ion production rates below 200 km altitude are consistent with the large observed daytime TEC increases. We showed that ion recombination occurs

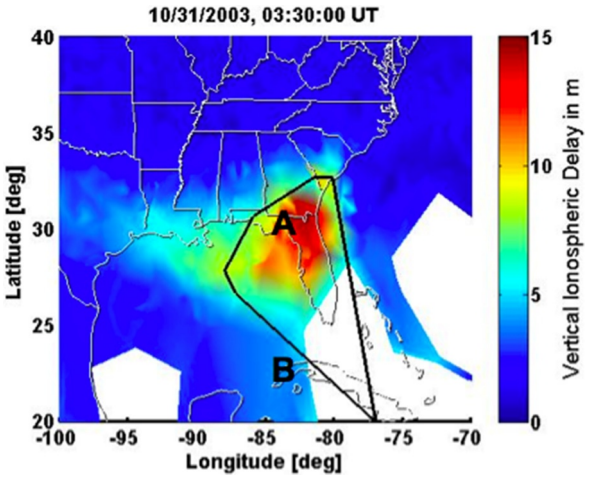

FIG. 6

The TEC enhancement known as the "Florida Effect" that occurred on October 31, 2003, as deduced from a ground network of GPS receivers. The region marked A is the expected shape of the enhanced region, based on GPS and ocean altimeter data. The region marked B is normal nighttime background.

relatively slowly for the uplifted plasma, consistent with the overall TEC increases (and with the observed increased altitude of the plasma, ascertained by comparing with ground-based TEC measurements, as discussed in Mannucci et al., 2005b). Daytime TEC increase is consistent with the Florida Effect if a sufficiently large quantity of plasma at high altitude might fail to recombine over a period of several hours. To assess plasma recombination rates, we use the IRI model in the vicinity of the Florida feature, comparing daytime and nighttime profiles. While the climatological IRI will not capture the storm-time features, it will capture the plasma recombination process versus altitude that occurs under typical conditions, which is of interest to us here.

The electron density profiles over Florida, day and night, and their ratio, are shown in Fig. 7. As expected, rapid recombination at altitudes lower than 225 km quickly reduces daytime plasma density by factors of 10 or greater. At altitudes of 500 km and above, the daytime plasma is reduced by only a factor of 3–4. Estimates of daytime TEC are 250.0 TECU near Florida (Fig. 1). Nighttime TEC reached ~80 TECU in the Florida Effect feature, lower by a factor of ~3 from the peak daytime value, which is consistent with slow upper altitude recombination. Of course, details of the processes that created the Florida Effect TEC feature are likely to be more complex than the picture offered here, including the causes of the structuring. These simplified calculations show it is plausible that the Florida Effect is a result of daytime plasma uplifted by long-duration PPEF.

5 CONCLUSIONS AND FUTURE OUTLOOK

The largest increases in ionospheric electron density and total electron content during intense geomagnetic storms are due to prompt penetration electric fields (PPEF), that tend to occur during the storm main phase, and can last for several hours. PPEF penetrating from high latitudes to the equatorial region

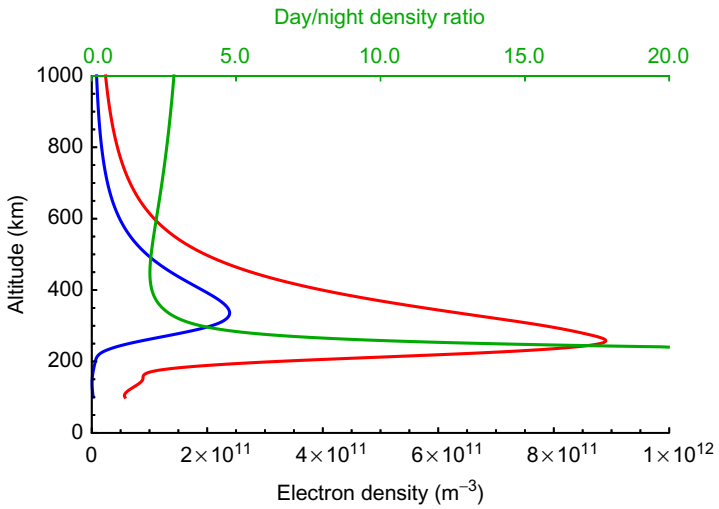

FIG. 7

Electron density profiles from the IRI-2016 model for nominal daytime conditions *(red trace)* on October 30, 2003, at 2120 UT (1600 LT solar), and nighttime conditions *(blue trace)* on October 31, 2003, at 0330 UT (2210 LT). The altitude-dependent ratio of the day to night density is plotted along the upper axis *(green)*.

create an ionospheric "superfountain" that vertically advects plasma from low to mid-latitudes via $\mathbf{E} \times \mathbf{B}$ drift. The large TEC increases that have been observed can be understood physically as a reduction of the plasma recombination process, whereby plasma created via photoionization at lower altitudes is rapidly raised to higher altitudes where recombination is much slower. The result is increased TEC and increased plasma densities at altitudes above 400 km. Combined with structured electric fields that may appear at subauroral latitudes, large electron density gradients are also a consequence of PPEF (see Chapter 23).

Extrapolating to the most extreme events, it is reasonable to expect increased electric field values and long-duration penetration (up to 24 h may be possible. An 18-h main phase is discussed in Chapter 7). Larger TEC values than observed during the October 2003 "Halloween" storms may be the result, perhaps spanning more than one day. We expect nonlinear effects (e.g., plasma heating) to play a role for the most extreme events, making simplistic extrapolation unreliable. Detailed modeling and theory are required to predict the consequences in more detail. Fortunately, the observations from 2003 show how rapidly TEC can grow, and it might get worse. Observations for this storm also show that at altitudes above 800 km, ion densities exceed neutral densities.

Applications that rely on predictable TEC spatial and temporal variations are likely to be affected by the aftermath of the large TEC increases, as occurred at night over Florida on October 31, 2003. The TEC magnitude and spatial variation of such structures are not currently understood, but it is likely, if they are indeed caused by remnant uplifted daytime plasma, that extreme geomagnetic storms will increase the severity of the effects resulting from such structures.

The prospect of catastrophic equatorial irregularities caused by extreme geomagnetic storms is not clear. Both suppression and enhancement of irregularities are associated with geomagnetic storms. Extreme events may bring over-shielding, PPEF, and fluctuating electric fields at low and middle

latitudes, particularly if magnetospheric ring current plasma is enhanced in a way conducive to such effects (see Chapter 10). Dusktime scintillation enhancement associated with rapidly changing Dst is plausible, another cause of increased low-latitude irregularities affecting postmidnight local times. However, because these are transient and localized enhancements, the consequences for extreme events are hard to predict.

Further work is required to investigate the role of ion-neutral coupling of rapidly uplifted plasma. A consequence may be noticeably increased satellite drag at altitudes above 500 km. Increased satellite drag is a known consequence of extreme space weather events due to thermospheric heating and circulation changes (see Chapter 21). Rapidly increased drag can lead to loss of satellite positions for hours or days. The thermospheric consequences of PPEF should be better understood in preparation for a future extreme event.

ACKNOWLEDGMENTS

This research was carried out at the Jet Propulsion Laboratory, California Institute of Technology, under a contract with the National Aeronautics and Space Administration. Useful discussions with Xing Meng (NASA Jet Propulsion Laboratory, California Institute of Technology) are acknowledged.

REFERENCES

Abdu, M.A., 2012. Equatorial spread F/plasma bubble irregularities under storm time disturbance electric fields. J. Atmos. Sol. Terr. Phys. 75–76 (C), 44–56. https://doi.org/10.1016/j.jastp.2011.04.024.

Anderson, D.N., 1973. A theoretical study of the ionospheric F region equatorial anomaly—I. Theory. Planet. Space Sci. 21 (3), 409–419. https://doi.org/10.1016/0032-0633(73)90040-8.

Bailey, G.J., Balan, N., 1996. A low-latitude ionosphere-plasmasphere model. In: Schunk, R.W. (Ed.), Solar-Terrestrial Energy Program: Handbook of Ionospheric Models, pp. 173–206.

Baron, M.J., Wand, R.H., 1983. Fregion ion temperature enhancements resulting from Joule heating. J. Geophys. Res. 88 (A5), 4114. https://doi.org/10.1029/ja088ia05p04114.

Basu, S., et al., 2001a. Ionospheric effects of major magnetic storms during the international space weather period of September and October 1999: GPS observations, VHF/UHF scintillations, and in situ density structures at middle and equatorial latitudes. J. Geophys. Res. 106 (A), 30389–30414. https://doi.org/10.1029/2001JA001116.

Basu, S., Basu, S., Groves, K.M., Yeh, H.C., Su, S.Y., Rich, F.J., Sultan, P.J., Keskinen, M.J., 2001b. Response of the equatorial ionosphere in the South Atlantic Region to the Great Magnetic Storm of July 15, 2000. Geophys. Res. Lett. 28 (18), 3577–3580. https://doi.org/10.1029/2001GL013259.

Basu, S., Basu, S., Rich, F.J., Groves, K.M., MacKenzie, E., Coker, C., Sahai, Y., Fagundes, P.R., Becker-Guedes, F., 2007. Response of the equatorial ionosphere at dusk to penetration electric fields during intense magnetic storms. J. Geophys. Res. 112 (A8), A08308–A08314. https://doi.org/10.1029/2006JA012192.

Bilitza, D., Altadill, D., Zhang, Y., Mertens, C., Truhlik, V., Richards, P., McKinnell, L.-A., Reinisch, B., 2014. The International Reference Ionosphere 2012 ? a model of international collaboration. J. Space Weather Space Clim. 4, A07–A13. https://doi.org/10.1051/swsc/2014004.

Brekke, A., Rino, C.L., 1978. High-resolution altitude profiles of the auroral zone energy dissipation due to ionospheric currents. J. Geophys. Res. 83 (A6), 2517–2524. https://doi.org/10.1029/JA083iA06p02517.

Carter, B.A., et al., 2014. Geomagnetic control of equatorial plasma bubble activity modeled by the TIEGCM with Kp. Geophys. Res. Lett. 41 (1), 5331–5339. https://doi.org/10.1002/2014GL060953.

Datta-Barua, S., Mannucci, A.J., Walter, T., Enge, P., 2008. Altitudinal variation of midlatitude localized TEC enhancement from ground- and space-based measurements. Space Weather 6 (10). https://doi.org/10.1029/2008SW000396.

Enge, P., Walter, T., Pullen, S., Kee, C., 1996. Wide area augmentation of the global positioning. Proceedings of the IEEE 84, 1063–1088.

Fejer, B.G., Scherliess, L., 1995. Time dependent response of equatorial ionospheric electric fields to magnetospheric disturbances. Geophys. Res. Lett. 22 (7), 851–854. https://doi.org/10.1029/95GL00390 (ISSN 0094–8276).

Hanson, W.B., Moffett, R.J., 1966. Ionization transport effects in the equatorial F region. J. Geophys. Res. Oceans 71 (23), 5559–5572. https://doi.org/10.1029/JZ071i023p05559.

Heelis, R.A., Sojka, J.J., David, M., Schunk, R.W., 2009. Storm time density enhancements in the middle-latitude dayside ionosphere. J. Geophys. Res. 114(A3). https://doi.org/10.1029/2008JA013690.

Huang, C.-S., Foster, J.C., Kelley, M.C., 2005. Long-duration penetration of the interplanetary electric field to the low-latitude ionosphere during the main phase of magnetic storms. J. Geophys. Res. 110. A11309, https://doi.org/10.1029/2005JA011202.

Huba, J.D., Joyce, G., Fedder, J.A., 2000. Sami2 is another model of the ionosphere (SAMI2): a new low-latitude ionosphere model. J. Geophys. Res. 105 (A), 23035–23054. https://doi.org/10.1029/2000JA000035.

Jursa, A.S. (Ed.), 1985. Handbook of Geophysics and the Space Environment. Air Force Geophysics Laboratory. National Technical Information Service, Springfield, VA, USA.

Kelley, M.C., 2009. The Earth's Ionosphere: Plasma Physics and Electrodynamics, second ed. Academic Press, New York.

Kelley, M.C., Ilma, R.R., Nicolls, M., Erickson, P., Goncharenko, L., Chau, J.L., Aponte, N., Kozyra, J.U., 2010. Spectacular low- and mid-latitude electrical fields and neutral winds during a superstorm. J. Atmos. Sol. Terr. Phys. 72 (4), 285–291. https://doi.org/10.1016/j.jastp.2008.12.006.

Kikuchi, T., Araki, T., Maeda, H., Maekawa, K., 1978. Transmission of polar electric fields to the equator. Nature 273 (5664), 650. https://doi.org/10.1038/273650a0.

Killeen, T.L., Hays, P.B., Carignan, G.R., Heelis, R.A., Hanson, W.B., Spencer, N.W., Brace, L.H., 1984. Ion-neutral coupling in the high-latitude F region evaluation of ion heating terms from dynamics explorer 2. J. Geophys. Res. 89 (A9), 7495–7508. https://doi.org/10.1029/JA089iA09p07495 (ISSN 0148–0227).

Mannucci, A.J., Wilson, B.D., Yuan, D.N., Ho, C.H., Lindqwister, U.J., Runge, T.F., 1998. A global mapping technique for GPS-derived ionospheric total electron content measurements. Radio Sci. 33 (3), 565–582. https://doi.org/10.1029/97rs02707.

Mannucci, A.J., Iijima, B.A., Lindqwister, U.J., Pi, X., Sparks, L., Wilson, B.D., 1999. GPS and ionosphere. In: -Stone, W.R. (Ed.), Review of Radio Science 1996–1999. Review of Radio …, New York.

Mannucci, A.J., et al., 2005a. Hemispheric daytime ionospheric response to intense solar wind forcing. In: Burch, J.L., Schulz, M., Spence, H. (Eds.), Inner Magnetosphere Interactions: New Perspectives From Imaging. Geophysical-Monograph 159, American Geophysical Union, New York, pp. 261–275. https://doi.org/10.1029/159GM20.

Mannucci, A.J., Tsurutani, B.T., Iijima, B.A., Komjathy, A., Saito, A., Gonzalez, W.D., Guarnieri, F.L., Kozyra, J.U., Skoug, R., 2005b. Dayside global ionospheric response to the major interplanetary events of October 29–30, 2003 "Halloween Storms" Geophys. Res. Lett. 32 (1). L12S02, https://doi.org/10.1029/2004GL021467.

Mannucci, A.J., Tsurutani, B.T., Abdu, M.A., Gonzalez, W.D., Komjathy, A., Echer, E., Iijima, B.A., Crowley, G., Anderson, D., 2008. Superposed epoch analysis of the dayside ionospheric response to four intense geomagnetic storms. J. Geophys. Res. 113. https://doi.org/10.1029/2007ja012732.

Mendillo, M., 2006. Storms in the ionosphere: patterns and processes for total electron content. Rev. Geophys. 44 (4), RG4001–RG4047. https://doi.org/10.1029/2005RG000193.

Mendillo, M., Klobuchar, J.A., 1975. Investigations of the ionospheric F region using multistation total electron content observations. J. Geophys. Res. 80 (4), 643–650. https://doi.org/10.1029/JA080i004p00643.

Meng, X., Komjathy, A., Verkhoglyadova, O.P., Yang, Y.M., Deng, Y., Mannucci, A.J., 2015. A new physics-based modeling approach for tsunami-ionosphere coupling. Geophys. Res. Lett. 42 (1), 4736–4744. https://doi.org/10.1002/2015GL064610.

Moffett, R.J., Hanson, W.B., 1965. Effect of ionization transport on the equatorial F-region. Nature 206 (4), 705–706. https://doi.org/10.1038/206705a0.

Nopper, R.W.J., Carovillano, R.L., 1978. Polar-equatorial coupling during magnetically active periods. Geophys. Res. Lett. 5 (8), 699–702. https://doi.org/10.1029/GL005i008p00699.

Picone, J.M., Hedin, A.E., Drob, D.P., Aikin, A.C., 2002. NRLMSISE-00 empirical model of the atmosphere: statistical comparisons and scientific issues. J. Geophys. Res. 107 (A12), https://doi.org/10.1029/2002JA009430 SIA 15-1–SIA 15-16.

Rees, D., 1995. Observations and modelling of ionospheric and thermospheric disturbances during major geomagnetic storms: a review. J. Atmos. Sol. Terr. Phys. 57 (12), 1433–1457. https://doi.org/10.1016/0021-9169(94)00142-b.

Richards, P.G., 2014. Solar cycle changes in the photochemistry of the ionosphere and thermosphere. In: Modeling the Ionosphere-Thermosphere System, vol. 89. John Wiley & Sons, Ltd., Chichester, pp. 29–37

Richmond, A.D., 1995. Ionospheric electrodynamics. In: Volland, H. (Ed.), In: Handbook of Atmospheric Electrodynamics, vol. 2. pp. 249–290.

Ridley, A.J., Deng, Y., Tóth, G., 2006. The global ionosphere–thermosphere model. J. Atmos. Sol. Terr. Phys. 68 (8), 839–864. https://doi.org/10.1016/j.jastp.2006.01.008.

Rishbeth, H., Garriott, O.K., 1970. Introduction to ionospheric physics. International Geophysics Series, vol. 14. Academic Press, New York.

Rothwell, P.L., Jasperse, J.R., 2006. Modeling the connection of the global ionospheric electric fields to the solar wind. J. Geophys. Res. 111 (A3), A03211–A03216. https://doi.org/10.1029/2004JA010992.

Schunk, R.W., Nagy, A.F., 2009. Ionospheres: Physics, Plasma Physics, and Chemistry, second ed. Cambridge University Press, New York.

Sparks, L., 2012. Addressing the influence of space weather on Airline Navigation. In: Proceedings of the 6th Annual Guidance and Control Conference; 5 Feb. 2012; Breckenridge, CO; United States.

Sparks, L., Blanch, J., Pandya, N., 2011a. Estimating ionospheric delay using kriging: 1. Methodology. Radio Sci. 46 (6), 1–13. https://doi.org/10.1029/2011RS004667.

Sparks, L., Blanch, J., Pandya, N., 2011b. Estimating ionospheric delay using kriging: 2. Impact on satellite-based augmentation system availability. Radio Sci. 46 (6), 1–10. https://doi.org/10.1029/2011RS004781.

Stephens, P., Komjathy, A., Wilson, B., Mannucci, A., 2011. New leveling and bias estimation algorithms for processing COSMIC/FORMOSAT-3 data for slant total electron content measurements. Radio Sci. 46 (6). https://doi.org/10.1029/2010RS004588.

Tsurutani, B., et al., 2004. Global dayside ionospheric uplift and enhancement associated with interplanetary electric fields. J. Geophys. Res. 109 (A). A08302, https://doi.org/10.1029/2003JA010342.

Tsurutani, B.T., Verkhoglyadova, O.P., Mannucci, A.J., Araki, T., Sato, A., Tsuda, T., Yumoto, K., 2007. Oxygen ion uplift and satellite drag effects during the 30 October 2003 daytime superfountain event. Ann. Geophys. 25 (3), 569–574. https://doi.org/10.5194/angeo-25-569-2007.

Tsurutani, B.T., Verkhoglyadova, O.P., Mannucci, A.J., Lakhina, G.S., Huba, J.D., 2012. Extreme changes in the dayside ionosphere during a Carrington-type magnetic storm. J. Space Weather Space Clim. 2, A05–A07. https://doi.org/10.1051/swsc/2012004.

Yeh, H.C., Su, S.Y., Heelis, R.A., 2001. Storm-time plasma irregularities in the pre-dawn hours observed by the low-latitude ROCSAT-1 satellite at 600 km altitude. Geophys. Res. Lett. 28, 685.

Zhu, J., Ridley, A.J., 2014. Modeling subsolar thermospheric waves during a solar flare and penetration electric fields. J. Geophys. Res. 119 (1), 10. https://doi.org/10.1002/2014JA020473.

Zhu, Q., Deng, Y., Maute, A., Sheng, C., Lin, C.Y., 2017. Impact of the vertical dynamics on the thermosphere at low and middle latitudes: GITM simulations. J. Geophys. Res. Space Phys. 122 (6), 6882–6891. https://doi.org/10.1002/2017JA023939.

FURTHER READING

Heroux, L., Cohen, M., Higgins, J.E., 1974. Electron densities between 110 and 300 km derived from solar EUV fluxes of August 23, 1972. J. Geophys. Res. 79 (34), 5237–5244. https://doi.org/10.1029/JA079i034p05237.

Hinteregger, H.E., Hall, L.A., Schmidtke, G., 1965. Solar XUV radiation and neutral particle distribution in July 1963 themosphere. pp. 1175; Space Research V. In: King-Hele, D.G., Muller, P., Righini, G. (Eds.), Proceedings of the Fifth International Space Science Symposium, Florence, May 12–16. 1964; Organized by the Committee on Space Research—COSPAR and the Italian Space Research Committee. North-Holland Publishing Company, Amsterdam, New York, 1965.

Mannucci, A.J., Tsurutani, B.T., Verkhoglyadova, O., Komjathy, A., Pi, X., 2015. Use of radio occultation to probe the high-latitude ionosphere. Atmos. Meas. Tech. 8 (7), 2789–2800. https://doi.org/10.5194/amt-8-2789-2015.